Helsinki University of Technology
CFD-group/ Laboratory of Applied Thermodynamics

MEMO No CFD/TERMO-9-96 DATE: May 24, 1996

TITLE

TEST CALCULATIONS OF VARIOUS TWO-EQUATION LOW REYNOLDS NUMBER TURBULENCE MODELS

AUTHOR(S)
Patrik Rautaheimo

ABSTRACT

Purpose of this work is compare different two-equation low Reynolds number turbulence model and their suitability to the different flow situations. There is comparison of old Chien $k-\epsilon$ model, cross-diffusion model and Gatski et al. ARSM. Flow simulations are applied for low Reynolds number channel flow, flow over flat plate, wall jet and curved duct.

MAIN RESULT

Implementation of the different turbulence models

PAGES
17

KEY WORDS
two-equation turbulence models, low Reynolds number, turbulence modeling.

APPROVED BY

Timo Siikonen May 24, 1996

1 Introduction

For a long time, so-called wall functions has been used for calculating wall-bounded turbulent flows. It means that boundary conditions can be applied to points in the fluid away from the boundaries and thereby avoid the problem of modeling the direct influence of viscosity. This procedure can be applied only for the situation in which the universal wall functions are valid. However, for a complex flow situations, the calculation of the flow variables must be extended next to the solid wall. Wall functions do not generally apply to the separation, stream line curvature, a system rotation or surfaces with mass or heat transfer. Thus, the low Reynolds number turbulence models have been applied in this work. To calculate near wall turbulence quantities means generally use damping functions in both Reynolds-stress models (RSM) and two equation models. These damping functions are depended the distance from the wall, unit wall normals or/and local shear stress in the closest solid wall. These relation are generally "ad hoc" in nature because they contain no turbulence physics and are calibrated based on the equilibrium turbulent boundary layer.

The desired turbulence model would be model that calculates values close to the wall without use of any damping functions. One of the such model is $k-\omega$ model of Wilcox [1]. However $k-\omega$ model has some undesired features. For example, it is very sensitive for a free stream turbulence. Other such model has been developed by UMIST group and also by Gatski et al. [2].

This paper is concerned with an evaluation some of existing two-equation, low Reynolds number turbulence model. Two models are ordinary isotropic two-equation models and one is explicid algebraic Reynolds-stress model (ARSM).

2 Methods

Three models, namely those of Chien [3], cross-diffusion modification of Yoon et al. [4] and Gatski et al. [2] with low Reynolds number correction by Abid et al. [5]. The first one is classical low Reynolds number $k-\epsilon$ model (CH), the second is Chien $k-\epsilon$ model with cross-diffusion modification (CD), and the third one is explicid ARSM (GS).

The $k-\epsilon$ model can be written as

$$\widetilde{\bar{\rho} u_i'' u_j''} = F(S_{ij}, W_{ij}, k, \epsilon, \mu_T) \tag{1}$$

$$\mu_T = c_\mu \, f_\mu \, \rho \, \frac{k^2}{\tilde{\epsilon}} \tag{2}$$

$$\epsilon = \tilde{\epsilon} + D \tag{3}$$

$$\frac{\partial \rho k}{\partial t} + \frac{\partial \rho u_i k}{\partial x_i} = \frac{\partial}{\partial x_i}\left[(\mu + \mu_T/\sigma_k)\frac{\partial k}{\partial x_i}\right] + P - \rho\,\epsilon \tag{4}$$

$$\frac{\partial \rho \tilde{\epsilon}}{\partial t} + \frac{\partial \rho u_i \tilde{\epsilon}}{\partial x_i} = \frac{\partial}{\partial x_i}\left[(\mu + \mu_T/\sigma_\epsilon)\frac{\partial \tilde{\epsilon}}{\partial x_i}\right] + c_{\epsilon\,1}\, f_1 \, \frac{\tilde{\epsilon}}{k} P - c_{\epsilon\,2}\, f_2 \, \frac{\rho \tilde{\epsilon}^2}{k} + c_{\epsilon\,3} c_\mu \frac{k^2}{\epsilon}\frac{\partial k}{\partial x_i}\frac{\partial}{\partial x_i}\left(\frac{\tilde{\epsilon}}{k}\right) + E \tag{5}$$

Table 1 summarizes functions and constants for a different turbulence models. Constants $c_{\epsilon\,1}$ and $c_{\epsilon\,3}$ can be determined from the other constants [4]

$$c_{\epsilon\,1} = c_{\epsilon\,2} - \frac{\kappa^2}{\sqrt{c_\mu}\sigma_\epsilon} \tag{6}$$

$$c_{\epsilon\,3} = \frac{1}{2}\left(-\frac{5}{\sigma_\epsilon} + \sqrt{\frac{24}{\sigma_\epsilon^2} - \frac{24 c_{\epsilon\,2}}{\sigma_k \sigma_\epsilon} + \frac{36}{\sigma_k^2}}\right) \tag{7}$$

Table. 1: Functions and constants.

Model	D	$\tilde{\epsilon}_w$-B.C.	c_μ	$c_{\epsilon\,1}$	$c_{\epsilon\,2}$	$c_{\epsilon\,3}$	σ_k	σ_ϵ
CH	$2\nu\frac{k}{y_n^2}$	$\frac{\partial\tilde{\epsilon}}{\partial y_n}=0$	0.09	1.44	1.92	0.0	1.0	1.3
CD	$2\nu\frac{k}{y_n^2}$	$\frac{\partial\tilde{\epsilon}}{\partial y_n}=0$	0.09	1.173	1.92	-1.26	1.0	0.75
GS.	0.0	$2\mu\left(\frac{\partial\sqrt{k}}{\partial y_n}\right)^2$	0.088	1.39	1.83	0.0	1.0	1.3

Model	f_μ	f_1	f_2	E
CH	$1.0-e^{-0.00115y^+}$	1.0	$1.0-0.22e^{-Re_T^2/36}$	$-2\mu(\tilde{\epsilon}/y_n^2)e^{-0.5y^+}$
CD	$1.0-e^{-0.00115y^+}$	1.0	$1.0-0.22e^{-Re_T^2/36}$	$-2\mu(\tilde{\epsilon}/y_n^2)e^{-0.5y^+}$
GS	1.0	1.0	$1.0-e^{-Re_y/12.5}$	0.0

Various Reynods numbers and dimensionless distances are defined as

$$Re_T = \frac{\rho\,k^2}{\mu\,\tilde{\epsilon}} \tag{8}$$

$$Re_y = \frac{\rho\sqrt{k}\,y_n}{\mu} \tag{9}$$

$$y^+ = \frac{\rho\,y_n u_\tau}{\mu} \tag{10}$$

$$u_\tau = = \sqrt{\tau_w/\rho} \tag{11}$$

and y_n is normal distance from the wall.

The production of turbulent kinetic energy P is exact

$$P = \bar{\rho}\widetilde{u_i''u_j''}\frac{\partial u_i}{\partial x_j} \tag{12}$$

and Reynolds stresses $\bar{\rho}\widetilde{u_i''u_j''}$ are modeled in CH and CD model by using Boussinesq approximation

$$\bar{\rho}\widetilde{u_i''u_j''} = -2\mu_T S_{ij} + \frac{2}{3}\delta_{ij}\rho\,k \tag{13}$$

where S_{ij} is the mean strain rate tensor

$$S_{ij} = \frac{1}{2}\left(\frac{\partial u_i}{\partial x_j}+\frac{\partial u_j}{\partial x_i}\right) \tag{14}$$

With explicit RSM model of Gatski and Speziale [2] (GS) the Reynolds stresses are given by

$$\begin{aligned}\bar{\rho}\widetilde{u_i''u_j''} &= \frac{2}{3}\rho\,k\,\delta_{ij} - \frac{6(1+\eta^2)\alpha_1}{3+\eta^2+6\xi^2\eta^2+6\xi^2}\rho\frac{k^2}{\epsilon}\Big[\Big(S_{ij}-\frac{1}{3}S_{kk}\delta_{ij}\Big)\\ &\quad +\alpha_4\frac{k}{\epsilon}\left(S_{ik}W_{kj}+S_{jk}W_{ki}\right)-\alpha_5\frac{k}{\epsilon}\Big(S_{ik}S_{kj}-\frac{1}{3}S_{kl}S_{kl}\delta_{ij}\Big)\Big]\end{aligned} \tag{15}$$

where

$$W_{ij} = \frac{1}{2}\left(\frac{\partial u_i}{\partial x_j}-\frac{\partial u_j}{\partial x_i}\right) \tag{16}$$

is the mean vorticity tensor. In Eq. (15) η and ξ are strain rate invariants defined by

$$\eta = \frac{1}{2}\frac{\alpha_3}{\alpha_1}(S_{ij}S_{ij})^{\frac{1}{2}}\frac{k}{\epsilon} \qquad \xi = \frac{1}{2}\frac{\alpha_2}{\alpha_1}(W_{ij}W_{ij})^{\frac{1}{2}}\frac{k}{\epsilon} \tag{17}$$

where α_1, α_2, α_3, α_4 and α_5 are the constants that assume the values of 0.107, 0.00250, 0.0190, 0.138 and 0.100, respectively [5].

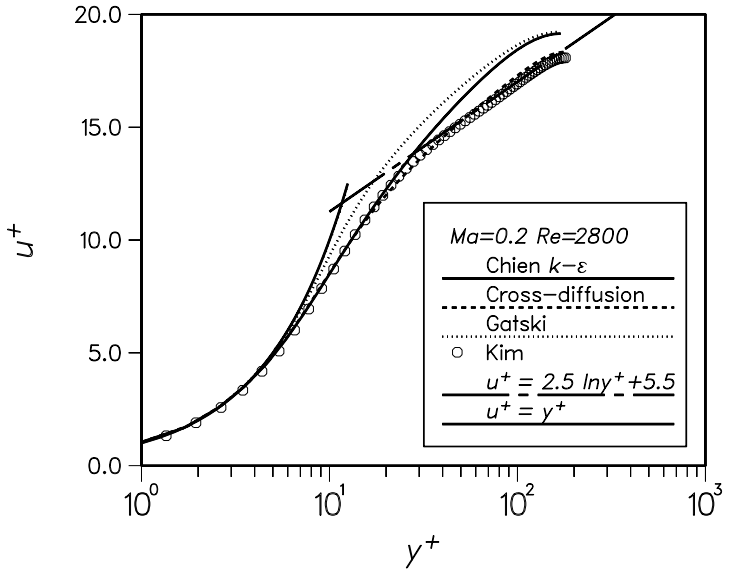

Fig. 1: Mean velocity profiles in wall coordinates.

3 Results

3.1 Channel Flow

The models were checked by calculating a fully developed flow in a plane channel. The results were compared with the DNS data of Kim et al. [6], and the Reynolds-stress budgets were compared with Mansour et al. [7] data. The DNS data is at $Re_m = \rho u_m \delta/\mu \approx 2\,800$ where u_m, δ and μ are the mean velocity, the channel half-width and molecular viscosity.

The mesh is rectangular 48×32. The height of the first row of cells is $\Delta y = 0.005\delta$ or $\Delta y^+ \approx 0.9$. Only half of the channel is modeled. The length of the computational mesh is 32δ. The calculations were performed using cyclic boundary conditions. After having a converged result, the solution was taken from the downstream boundary and utilized as the upstream boundary condition of the next run.

The velocity profiles are compared in Fig.1 in terms of u^+, which is a universal dimensionless velocity defined as $u^+ = u/u_\tau$, where $u_\tau = \sqrt{\tau_w/\rho}$ is a friction velocity. The velocity profiles in a viscous sublayer agree well with DNS and universal profiles. The velocity profiles are not completely satisfactory in outer layers. Only the CD model gives excellent results in this simply case. The turbulent stress can be seen in Fig.2. It can be seen that CH and GS under predict the skin-friction and that is also the reason why velocity distributions are so badly estimated. The turbulent stress should be almost straight line between $y^+ = 50 \rightarrow 180$. None of the model has that feature. The kinetic energy of turbulence is shown in Fig.3. It can been seen that CH and CD models estimate the peak of the kinetic energy of turbulence well in a close wall region whereas GS model do not estimate it at all. It also should be noted that GS model gives no kinetic energy of turbulence at the very close to the wall ($y^+ < 4$). Non-isotrophy of the Reynolds stresses in GS model is shown in Fig.3. It can be seen that the Reynolds-stresses are very close to each other.

3.2 Flat Plate

The next test case was the flow over a flat plate with high free-stream turbulent intensity. The test case was taken from ERCOFTAC Fluid Dynamics Database WWW Services (`http://fluindigo.mech.surrey.ac.uk/`) kept by P. Voke. Measurements were made by John Coupland (Rolls-Royce).

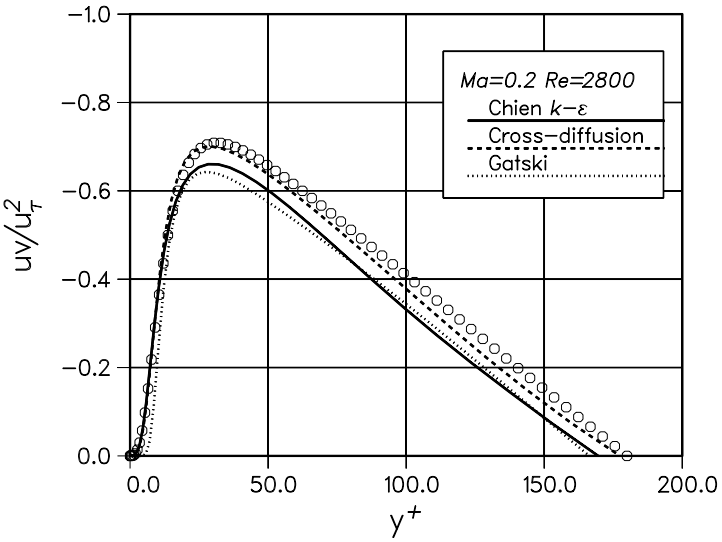

Fig. 2: Comparison of the calculated turbulent stress and the DNS-data in a plane channel.

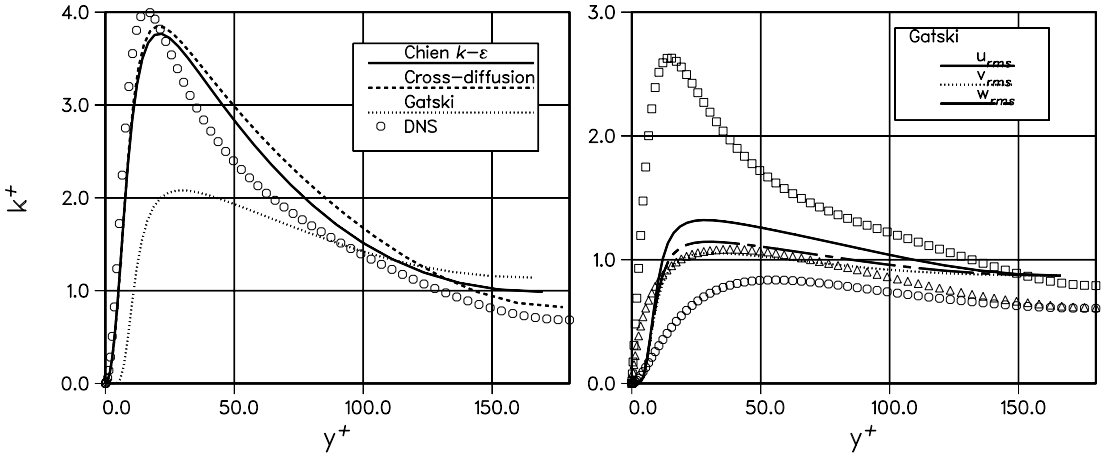

Fig. 3: Comparison of the calculated kinetic energy of turbulence and comparison of Reynolds stress components with Gatski model.

Inlet velocity was 9.4m/s and the pressure gradient was zero. Measurements were made down to $x = 1.495$m that correspond to $Re_x \approx 940\,000$. Upstream turbulence intensity (at the beginning of the flat plate) was $Tu = 6.0\%$ where turbulence level is defined as $Tu = \sqrt{\frac{1}{3}\widetilde{u_i'' u_i''}}/U = \sqrt{\frac{2}{3}k}/U$. Dissipation is set so that decay of free-stream turbulence is in balance. Also dissipation values could have been changed and that would have had some effect in boundary layer. These effects were not studied. Resulting kinetic energy of turbulence, dissipation and turbulence coefficient (μ_T/μ) at the free-stream can be seen in Fig.4. It can be seen that GS model has different behaviour than others. This is due to fact that $c_{\epsilon 2}$ has different values. The models are similar in a free-stream where there are no gradients. For example the turbulent kinetic energy and the dissipation equation reduced in following form if stream wise diffusion is neglected

$$\frac{\partial^2 k}{\partial x^2} = \frac{C_{\epsilon 2}}{k}\left(\frac{\partial k}{\partial x}\right)^2 \tag{18}$$

where x is along to the flow.

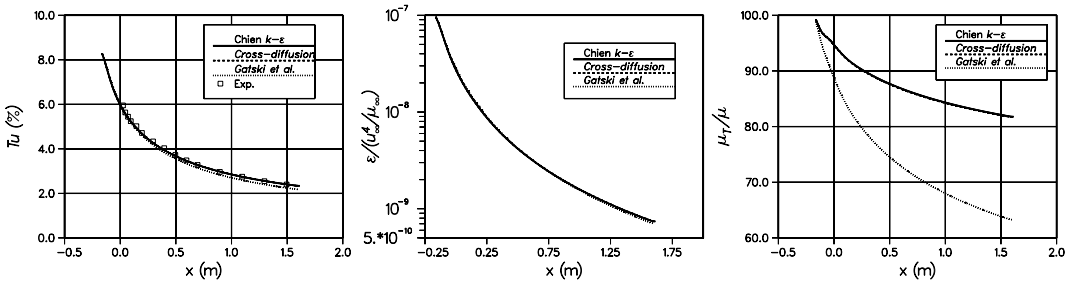

Fig. 4: Decay of turbulence quantities at free-stream along x-axis.

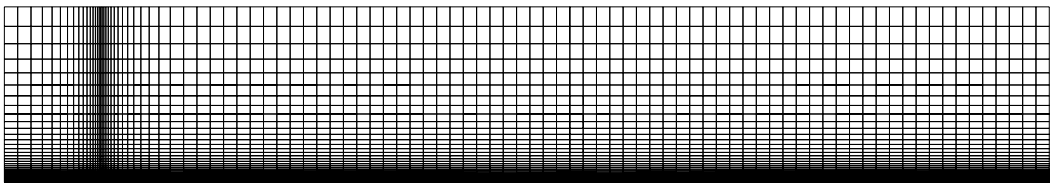

Fig. 5: Grid of the flat plate calculations.

The calculation was started 16cm before the flat plate. The length of the flat plate was 1.6m. The height was 30cm and the height of the first row of cells was 2.5×10^{-5}m that is equal to $y^+ \approx 0.7$ at most of the domain (at the leading edge $y^+ = 2.1$). Grid is heavily clustered to the wall expect the first three rows are kept constant. The ratio between neighboring cells is $\Delta y_{n+1}/\Delta y_n = 1.125$. The grid size is 96×64. The grid can be seen in Fig. 5.

Inlet conditions were uniform velocity distribution and pressure is extrapolated from the computational domain. Symmetry conditions were applied before the flat plate. At the flat plate, the velocities and kinetic energy of turbulence were set zero. Dissipation was threated as written in Table 1. Zero gradients were assumed at the outlet. The pressure was given. Boundary parallel to the wall was assumed to be zero gradient, except u-velocity component and pressure was given. The second-order upwind scheme was used with Roe's flux splitting [8].

Universal boundary layer parameters are shown in Fig.6. Boundary layer parameters are in figure from left to right: friction coefficient c_f, boundary layer thickness at point where velocity is 99% of the free stream velocity δ_{99}, displacement thickness δ^*_{99}, momentum thickness θ and shape function $H = \delta^*_{99}/\theta$. These variables are defined as

$$c_f = \tau_w / \left(\frac{1}{2}\rho U_e^2\right) \tag{19}$$

$$\delta^* = \int_0^{\delta_{99}} (1 - \frac{u(y)}{U_e}) dy \tag{20}$$

$$\theta = \int_0^{\delta_{99}} \frac{u(y)}{U_e}(1 - \frac{u(y)}{U_e}) dy \tag{21}$$

where U_e velocity at the edge of the boundary layer. Overall performance of the friction coefficient is the best for CD model, but a interesting feature is that GS model gets the transition in a right place. Even it is not strong enough this is promising because no transition model were used. Maybe CH model also get the transition but it begins too early and it is too weak. At the begin of the flat plate all the models get too low friction coefficients but they recover at the station $x \approx 0.8m$. The boundary layer thickness is best estimated by GS model. Displacement and momentum thickness are estimated very well by CD model except at the beginning of the flat plate, where GS performs very well. This is

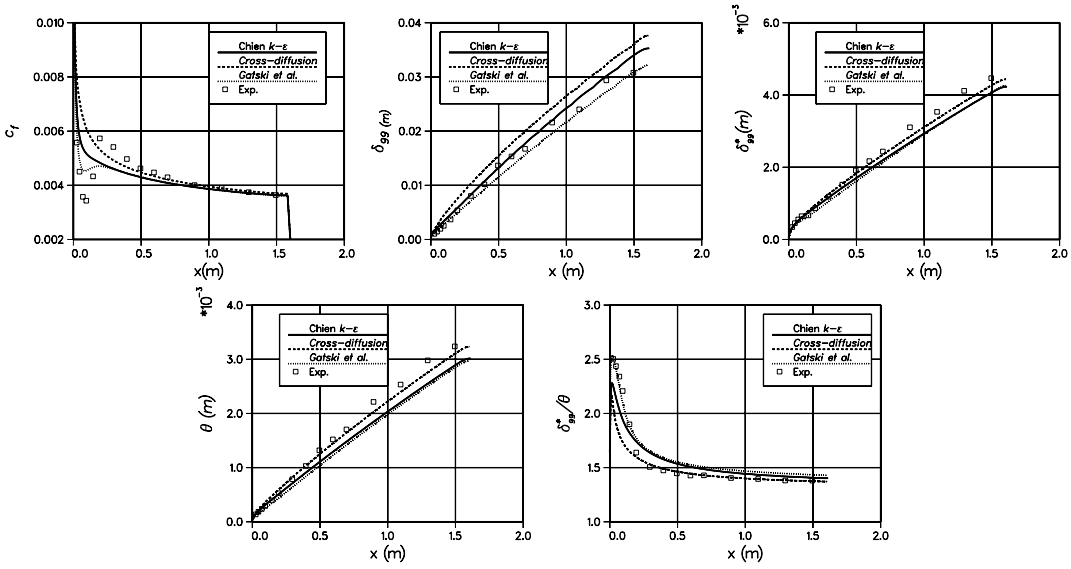

Fig. 6: Universal boundary layer parameters. From left to right: friction coefficient, boundary layer thickness, displacement thickness, momentum thickness and shape function.

due to fact that GS model predict the laminar part at the beginning of the boundary layer.

Velocity profiles are shown in Fig.7. In the figure y-axis is the nondimensional velocity ($u^+ = u/u_\tau$) and x-axis is nondimensional distance from solid wall (y^+). Symbols are same with Fig.6 with models and dashed-doted line is universal velocity distributions in two regions, viscous shear layer and overlap layer. Those are defined as

$$u^+ = y^+ \quad \text{when } y^+ < 5 \tag{22}$$

$$u^+ = \frac{1}{0.4}\ln y^+ + 5.5 \quad \text{when } 35 < y^+ < 350 \tag{23}$$

$$\tag{24}$$

It can be seen in Fig.7 same thing as was seen in Fig.6. The GS model predicts the laminar profile beginning of the flat plate as CD is turbulent all way down. However after transition, say station $x = 0.195$m, the CD model performs superiorly agains others. At the last station velocity profiles are similar with different models.

Turbulence intensities ($Tu = \sqrt{\frac{2}{3}k}/U_e$) profiles are shown in Fig.8. None of the models estimate the kinetic energy levels well. Worst is the GS model, that is surprising, because it is the newest model and performed well in velocity profiles. Also it is well seen in profiles that GS model predict zero degree of turbulence up to $y^+ \approx 3$ from the wall.

3.3 Wall Jet

Next test case was a two-dimensional plane wall jet enters along the bottom of a large pool, through a thin slot. Results were compared agains LDV measurements [9].

Flow was entering in 1cm slot. The dimensions of the pool was 7.45m × 1.35m. The inlet velocity was 1m/s that correspond the inlet Reynolds number $Re = U_0 b/\nu = 10\,000$. Kinematic viscosity of water at 18^{o}C is $\nu = 1.05 \times 10^{-6}\mathrm{m}^2/\mathrm{s}$. This case was also one of test cases of 5th ERCOFTAC-IAHR Workshop on Refined Modelling of Turbulent Flows (1996). At the inlet, only u velocity and u fluctuation component were measured. At the inflow slot, the measured velocity profile is specified. Since w' (rms) and actually also v' (rms) are unknown at the inlet, their mutual contribution to the turbulence kinetic energy k is approximated to be equal to the contribution of u' (rms) alone. Thus, k is approximated as $0.65\overline{u'u'}$ ($v' = 0$ and $w' \approx 0.3u'$). Dissipation is calculated so that the dissipation equation is

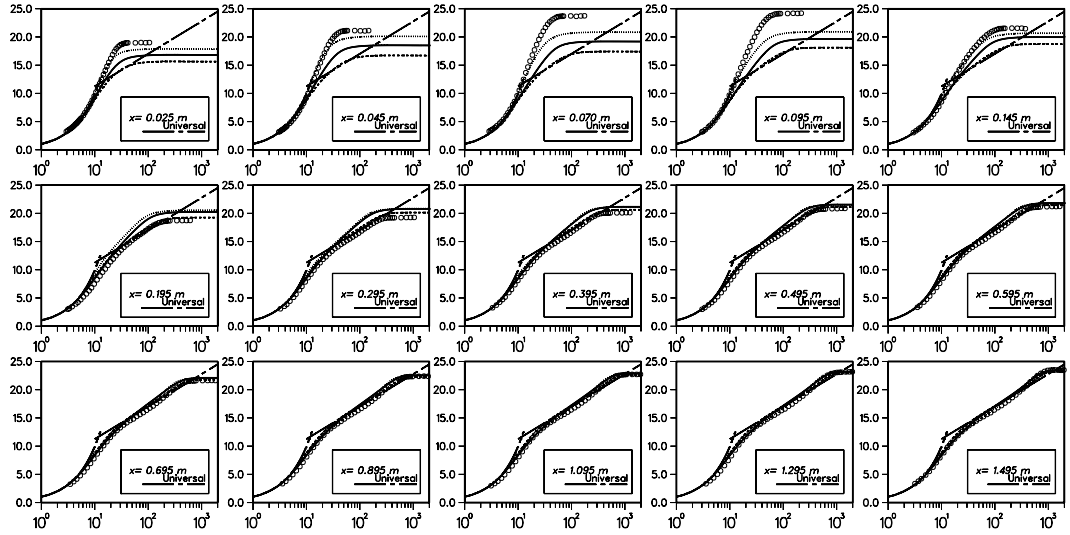

Fig. 7: Velicity profiles for different down-stream stations. Solid line is CH, dash line is CD, doted line is GS, dashed-doted line is universal velicity and the dots are the experiments.

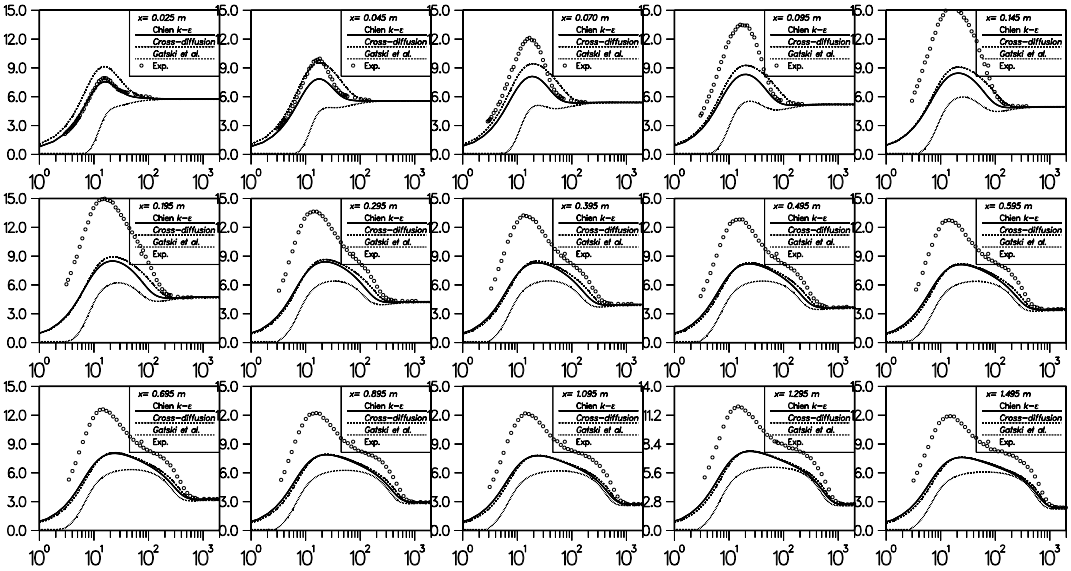

Fig. 8: Turbulent intensity profiles for different down-stream stations.

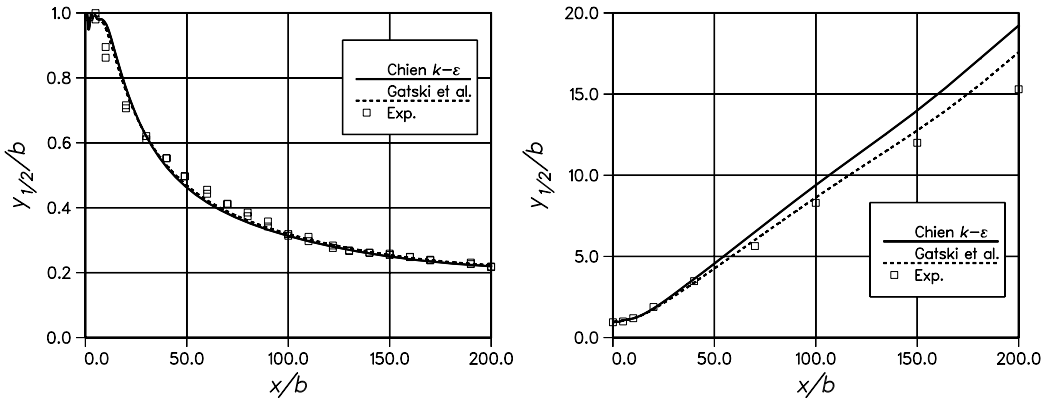

Fig. 9: Maximum velocity and sperthing rate of the jet.

in balance with the distributions of velocity and kinetic energy of turbulence. By repeating the calculations with several inflow ϵ-distributions, the flow field was found to be insensitive to the inlet ϵ-conditions. If given turbulent kinetic energy values were used the flow had a oscillation at the first measurement stations. Ten times larger fluctuating values did not have an effect after about 10 slot height, but larger fluctuating values have a significant effect in stability of the problem. With higher fluctuation values the flow was stable also close to the jet entrance. In the final calculation the larger values were used. At the outflow slot, the upper right corner of the pool, the static pressure is fixed. Mirror condition were used at the surface of the pool.

An orthogonal grid is used to model the whole pool. The grid consists of 64 cells in the direction of the jet (i) and 80 cells in the jet normal direction (j). The grid is heavily clustered in j-direction to the pool bottom wall and 32 cells were placed inside the inlet slot height. There is also clustering in i-direction so that the majority of the cells in the i-direction lie inside the area of interest. Near-wall cells in j-direction extend to a distance of about 3×10^{-5}m and in i-direction extend to a distance of about 1.1×10^{-3}m

The spreading of the jet was totally wrong with the CD model. After some test modifications results were not obtained with that model. Only CH and GS model will be presented. Modifying CD model to estimate the jet correctly is leaved to be the future work.

Maximum velocity and the spreading rate of the jet can be seen in Fig.9. GS model does little bit better than CH model. Various profiles for different stations can be seen in Appendix A. These profiles indicates that both models work pretty well. GS model does little bit better again in these figures. For first stations, both model work quite badly. This is because of the transition that takes place close to entrance of the jet. After station 03 both models simulate flow very well.

3.4 Curved rectangular duct

Last test case was flow in a 90^o curved duct of rectangular cross-section with aspect ratio 6. Experiments were done by Kim et al. [10]. How-wire velocity measurements have been carried out using a miniature X-wire probe for the turbulence quantities. Mean velocity measurements have been carried out using a five-hole pressure probe of a diameter of 3mm. This case was also one of test cases of 5th ERCOFTAC-IAHR Workshop on Refined Modelling of Turbulent Flows (1996).

Duct was with two straight and one curved sections. In Fig.10 can be seen geometry of the duct. Also measurement stations (U1, U2, 15, 45, 75, D1 and D2) are specified in the figure. Inlet conditions were given in station U1. Only dissipation must be approximated. It was approximated so that the dissipation equation is in balance with the distributions of velocity and kinetic energy of turbulence. The inlet velocity was 16m/s that correspond the inlet

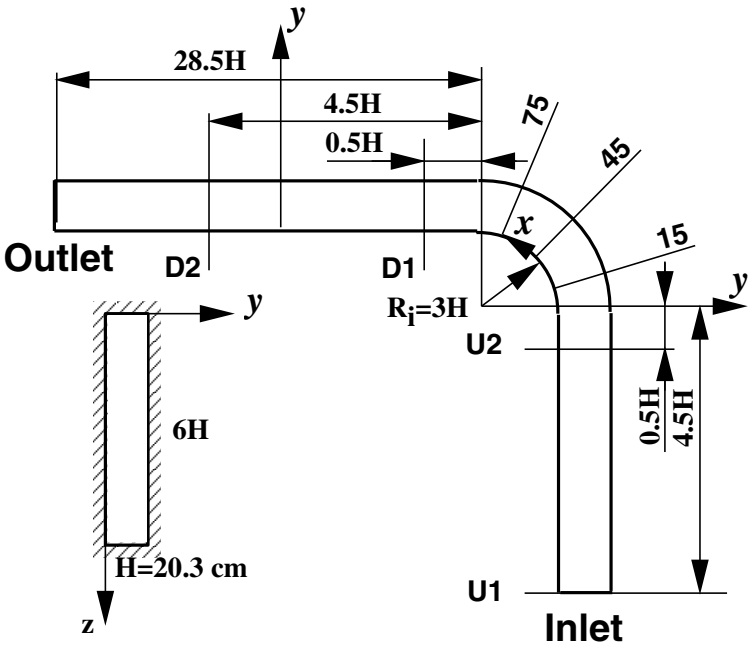

Fig. 10: Geometry of the curved duct.

Reynolds number $Re = U_0 b/\nu = 224\,000$. Kinematic viscosity of air is $\nu = 1.455 \times 10^{-5}\mathrm{m}^2/\mathrm{s}$. The duct is interesting test case because there was turbulence driving vortices because of nonisotropy of Reynolds stresses and also pressure driving vortices in the curved section.

An orthogonal grid is used to model the whole duct. Mesh consists of 393 216 cells with a total dimension of $64 \times 48 \times 128$. From U1 to the bending there is 48 cells, at the bending there is 48 cells and after bending to the outlet there is 32 cells. The computational domain is divided into 4 blocks in order to utilize parallel computation. The calculations begin in station U1 and ends in $x = 28.5H$. Near-wall cells in y and z direction extend to a distance of about 4×10^{-5}m.

Pressure distribution along the duct symmetry plane is shown in Fig.11. Both models show good agreement with experiments. Friction coefficient from inner wall to outer wall is presented in Fig.12. Friction coefficients are not so well estimated as pressure coefficients. Expecially close to the corner models have problems to estimate right friction coefficients.

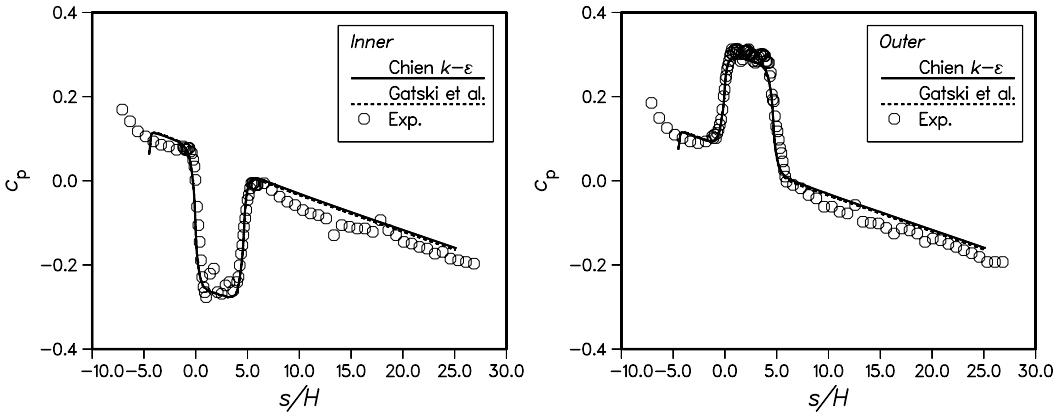

Fig. 11: Pressure distribution along the duct symmetry plane.

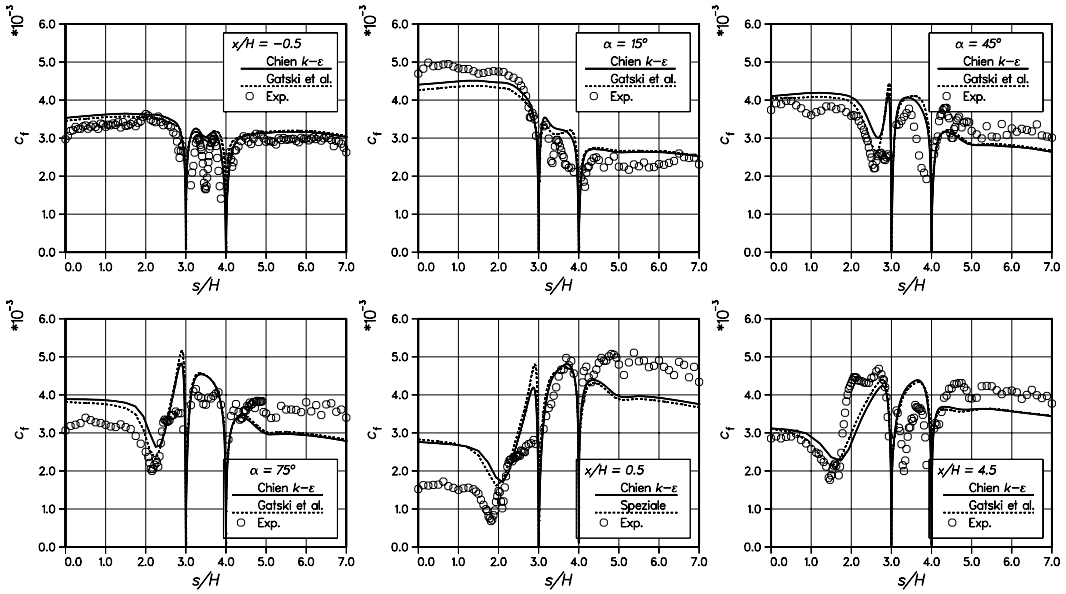

Fig. 12: Friction coefficient from inner wall to outer wall.

The bottom wall is badly estimated all most in every stations. Velocity fringes for GS model can be seen in Fig.13. It should be noted that colors are not exactly same for experiments and calculations all though the number of colors are same. Fringes of kinetic energy of turbulence for GS model can be seen in Fig.14. Velocity and kinetic energy of turbulence distributions were very close to each other with GS and CH models, and thus no figures of CH model is printed. Kinetic energy of turbulence is not so well estimated at the corners. Secondary motion and turbulent viscosity μ_T/μ is presented in Fig.15. Only small differences can be seen between models. Although experiments are not shown here the GS model make bit better estimate for secondary motion.

4 Discussion

There is no big differencies between models in these calculations. GS model estimates flow field best of these three models. Because its nonisotrophy, it is promising model for rotating flows. CD model has problems with spreading of the jet but it estimates close wall behaviour very well. This might be interest of the future research. For simple cases, channel flow, boundary layer and wall jet, all models performed well, but for more complicated case, in the curved duct, models have big difficulties.

All thought none of the model were not made to simulate transition, the CH and GS models predict transition close to the right place in the boundary layer problem. Transition were not strong enough.

References

[1] Wilcox, D., *Turbulence Modeling for CFD.* La Canada: DCW Industries, Inc., 1993. ISBN 0–9636051–0–0.

[2] Gatski, T. and Speziale, C., "On explicit algebraic stress models for complex turbulent flows," *Journal of Fluid Mechanics*, Vol. 254, 1993, pp. 59–78.

[3] Chien, K.-Y., "Predictions of Channel and Boundary-Layer Flows with a Low-Reynods-Number Turbulence Model," *AIAA Journal*, Vol. 20, Jan 1982, pp. 33–38.

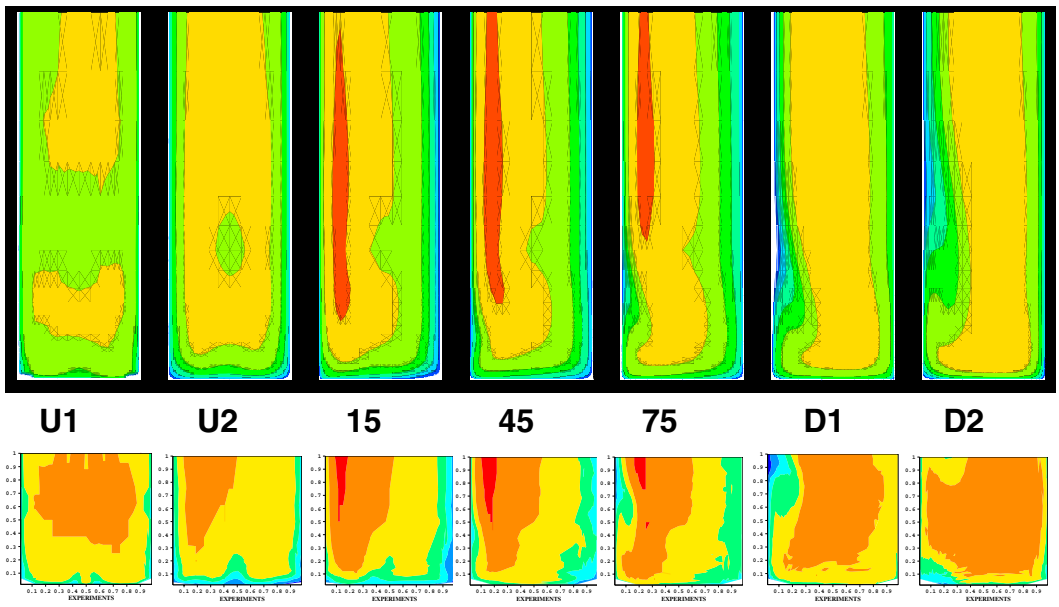

Fig. 13: Velocity fringes for GS model. Upper is GS model and lower experiments.

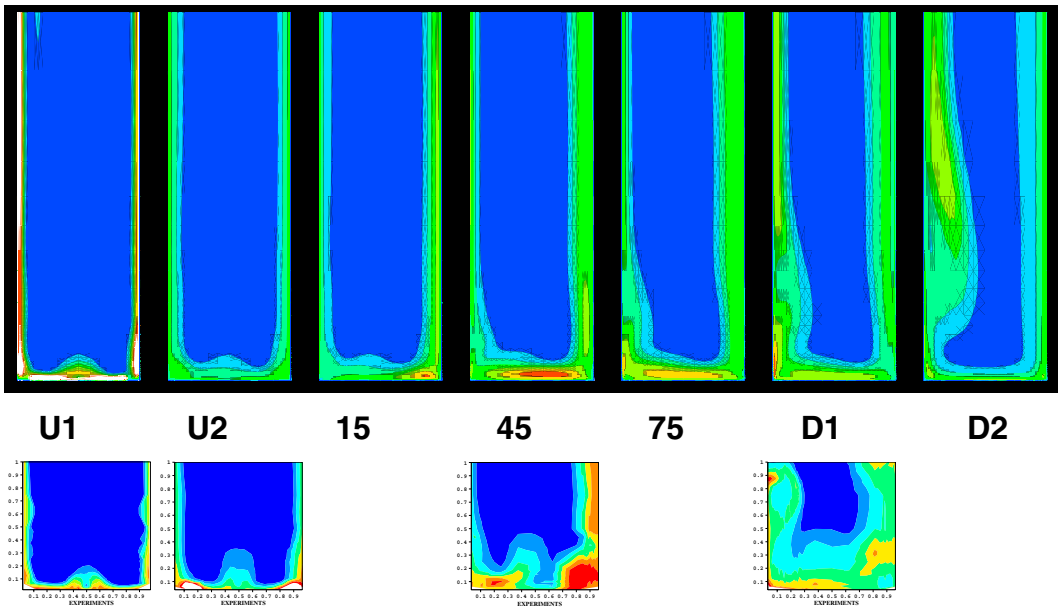

Fig. 14: Fringes of kinetic energy of turbulence for GS model. Upper is GS model and lower experiments.

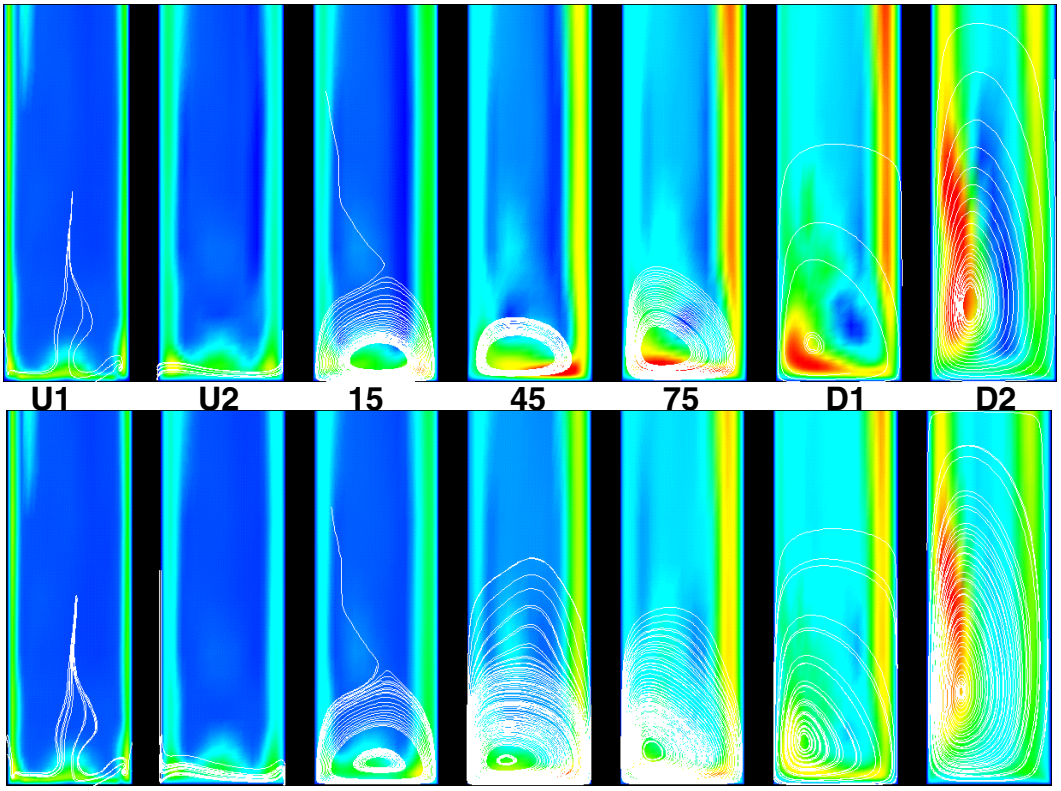

Fig. 15: Secondary motion in CH (upper) and GS (lower) model. Colors are turbulent viscosity μ_T/μ, blue color correspond zero value and red color 350.

[4] Yoon, B. and M.K., C., "Computation of Compression Ramp Flow with a Cross-Diffusion Modified $k-\epsilon$ Model," *AIAA Journal*, Vol. 33, No. 8, 1995, pp. 1518–1521.

[5] Abid, R., Rumsey, C., and Gatski, T., "Prediction of Nonequilibrium Turbulent Flows with Explicit Algebraic Stress Models," *AIAA*, Vol. 33, No. 11, 1995, pp. 2026–2031.

[6] Kim, J., Moin, P., and Moser, R., "Turbulence Statistics in Fully Developed Channel Flow at Low Reynolds Number," *Journal of Fluid Mechanics*, Vol. 177, 1987, pp. 133–166.

[7] Mansour, N., Kim, J., and Moin, P., "Reynolds-stress and Dissipation-rate Budgets in a Turbulent Channel Flow," *Journal of Fluid Mechanics*, Vol. 194, 1988, pp. 15–44.

[8] Roe, P., "Approximate Riemann Solvers, Parameter Vectors, and Difference Schemes," *Journal of Computational Physics*, Vol. 43, 1981, pp. 357–372.

[9] Karlsson, R., Eriksson, J., and Persson, J., "LDV Measurements in a Plane Wall Jet in a Large Enclosure," in *6th International Symposium on Applications of Laser Techniques to Fluid Mechanics*, (Lisbon, Portugal), pp. 1.5.1–1.5.6, July 1992.

[10] Kim, W. and Patel, V., "Origin and Decay of Longitudinal Vortices in Developing Flow in a Curved Rectangular Duct," *Journal of Fluid Engineerin*, Vol. 116, March 1994, pp. 45–52.

A Results for wall jet

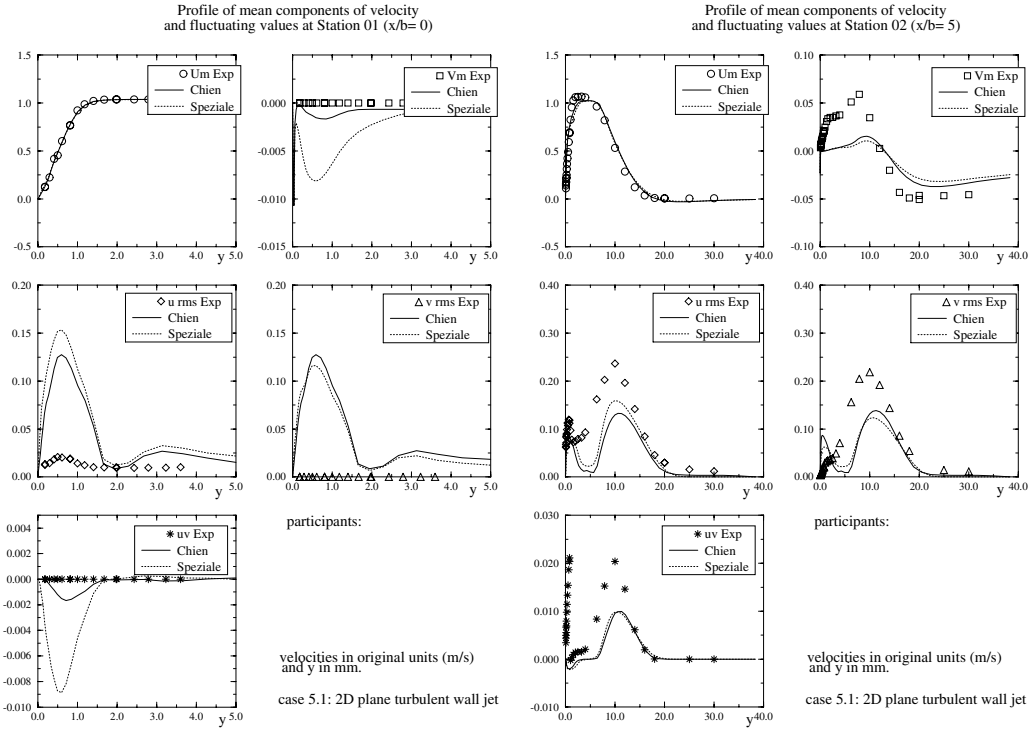

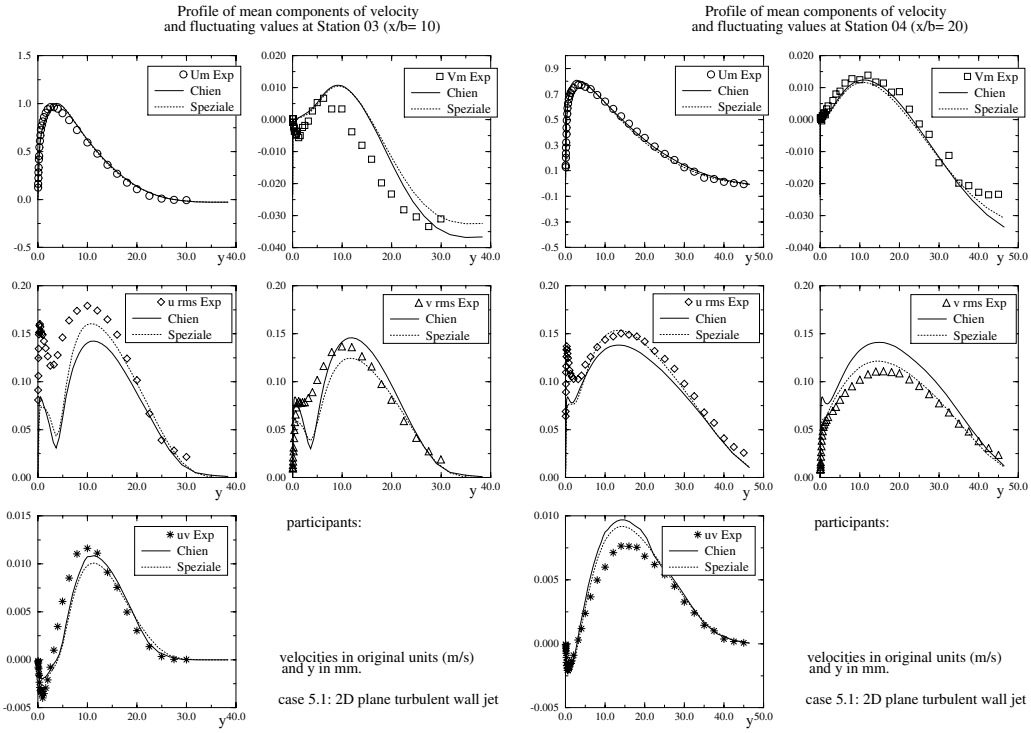

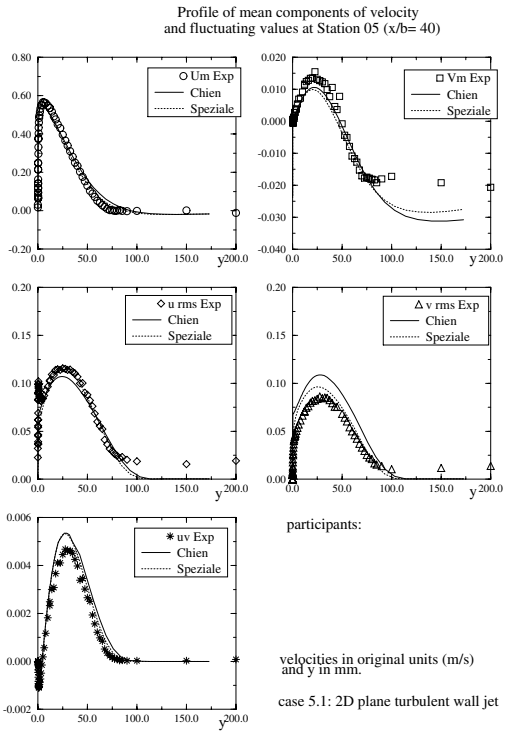

participants:

velocities in original units (m/s)
and y in mm.

case 5.1: 2D plane turbulent wall jet

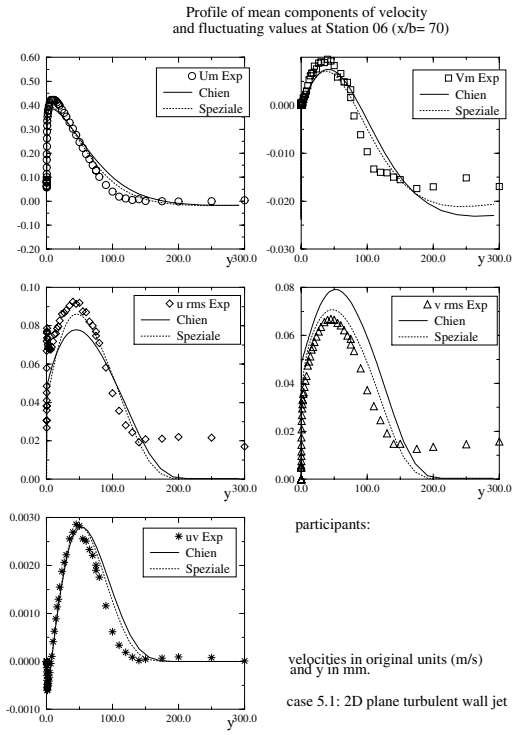

participants:

velocities in original units (m/s)
and y in mm.

case 5.1: 2D plane turbulent wall jet

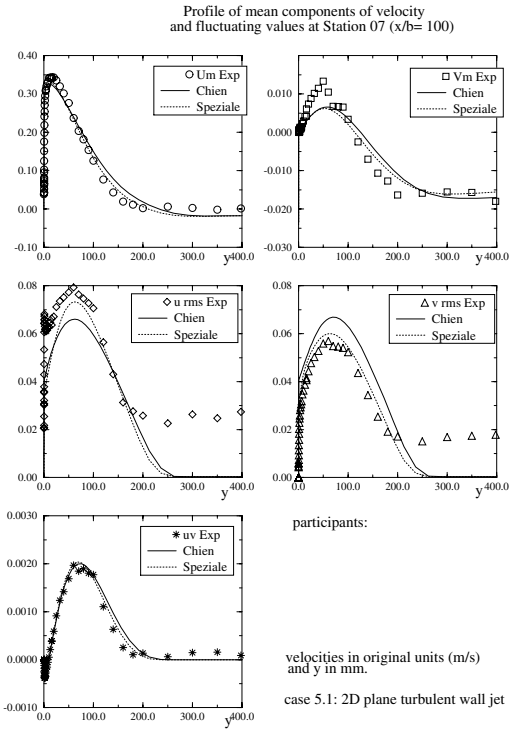

participants:

velocities in original units (m/s)
and y in mm.

case 5.1: 2D plane turbulent wall jet

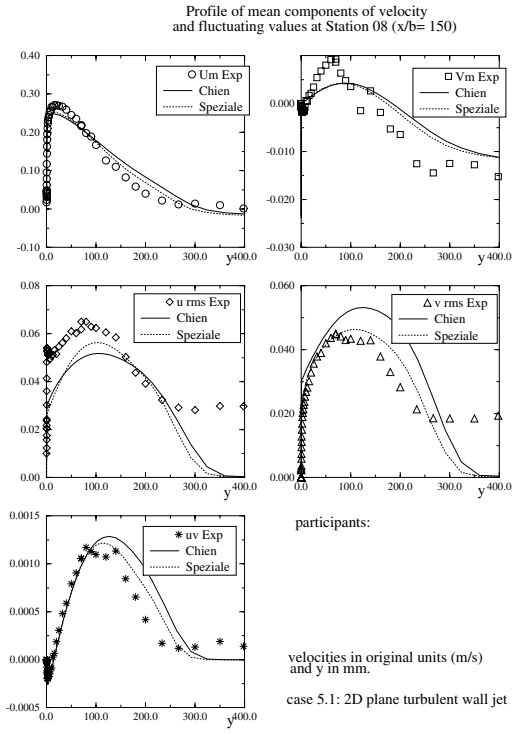

participants:

velocities in original units (m/s)
and y in mm.

case 5.1: 2D plane turbulent wall jet

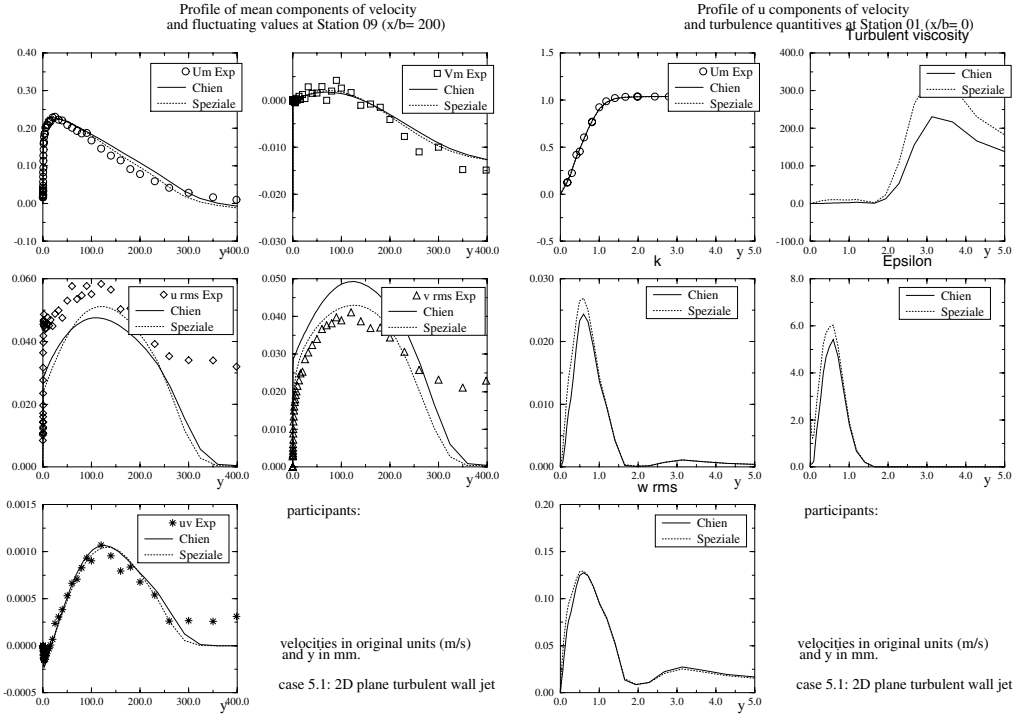
Profile of mean components of velocity
and fluctuating values at Station 09 (x/b= 200)
Um Exp
Vm Exp
u rms Exp
v rms Exp
uv Exp
Chien
Speziale
y
participants:
velocities in original units (m/s)
and y in mm.
case 5.1: 2D plane turbulent wall jet
Profile of u components of velocity
and turbulence quantitives at Station 01 (x/b= 0)
Um Exp
Turbulent viscosity
k
Epsilon
w rms
Chien
Speziale
participants:
velocities in original units (m/s)
and y in mm.
case 5.1: 2D plane turbulent wall jet

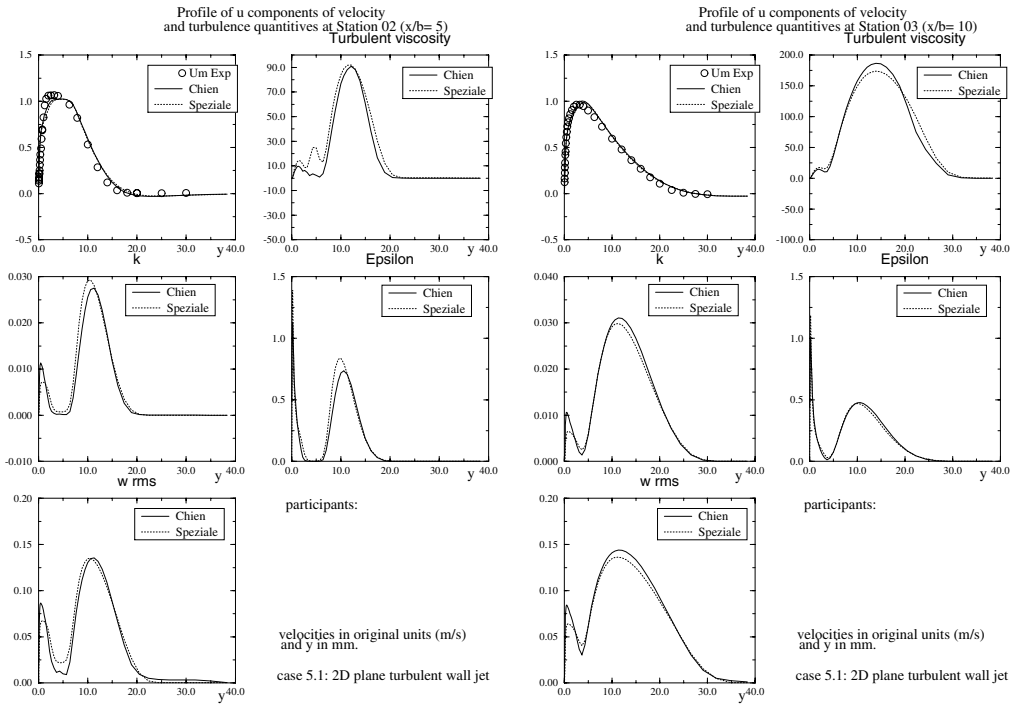
Profile of u components of velocity
and turbulence quantitives at Station 02 (x/b= 5)
Um Exp
Turbulent viscosity
k
Epsilon
w rms
Chien
Speziale
y
participants:
velocities in original units (m/s)
and y in mm.
case 5.1: 2D plane turbulent wall jet
Profile of u components of velocity
and turbulence quantitives at Station 03 (x/b= 10)
Um Exp
Turbulent viscosity
k
Epsilon
w rms
Chien
Speziale
participants:
velocities in original units (m/s)
and y in mm.
case 5.1: 2D plane turbulent wall jet

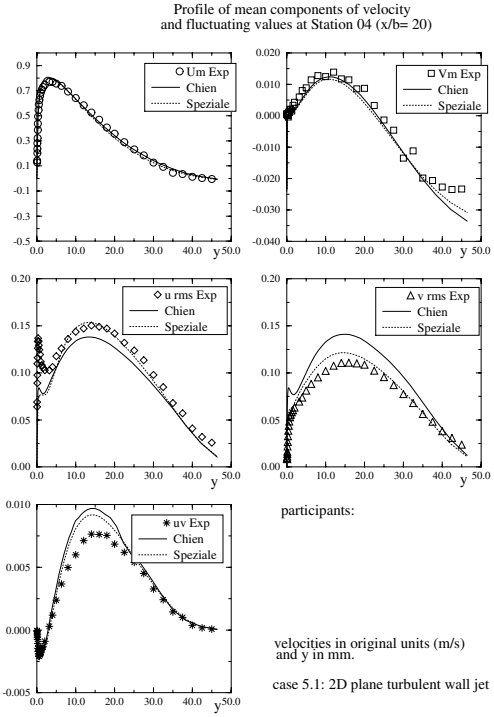

participants:

velocities in original units (m/s)
and y in mm.

case 5.1: 2D plane turbulent wall jet

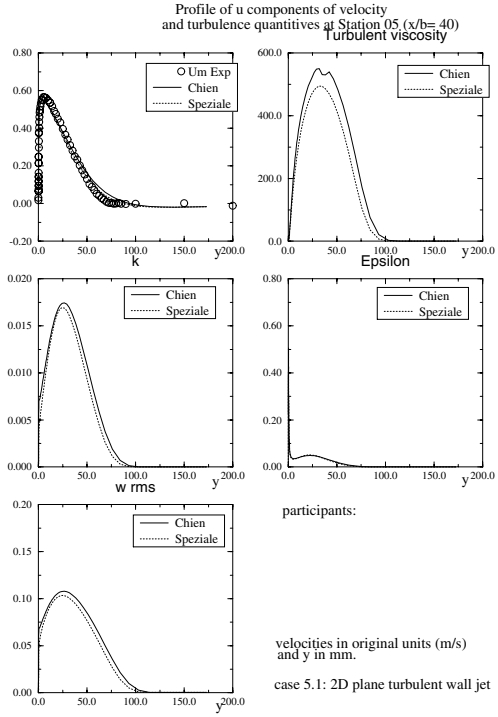

participants:

velocities in original units (m/s)
and y in mm.

case 5.1: 2D plane turbulent wall jet

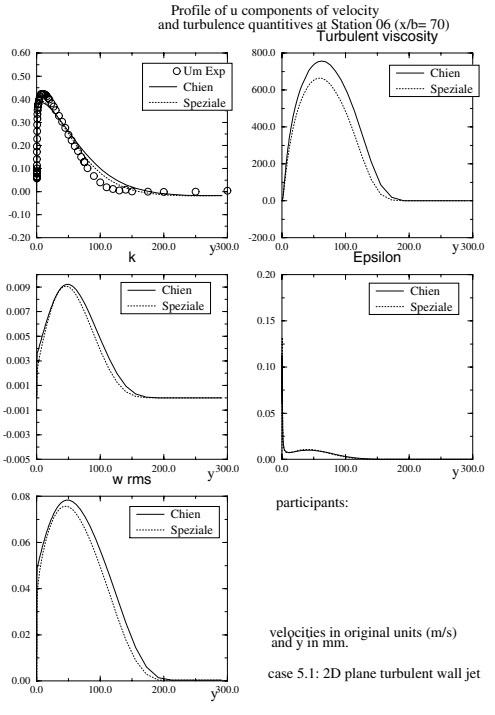

participants:

velocities in original units (m/s)
and y in mm.

case 5.1: 2D plane turbulent wall jet

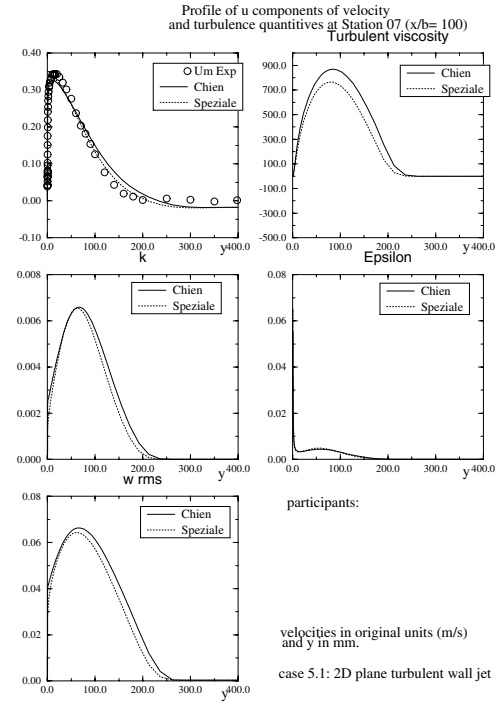

participants:

velocities in original units (m/s)
and y in mm.

case 5.1: 2D plane turbulent wall jet

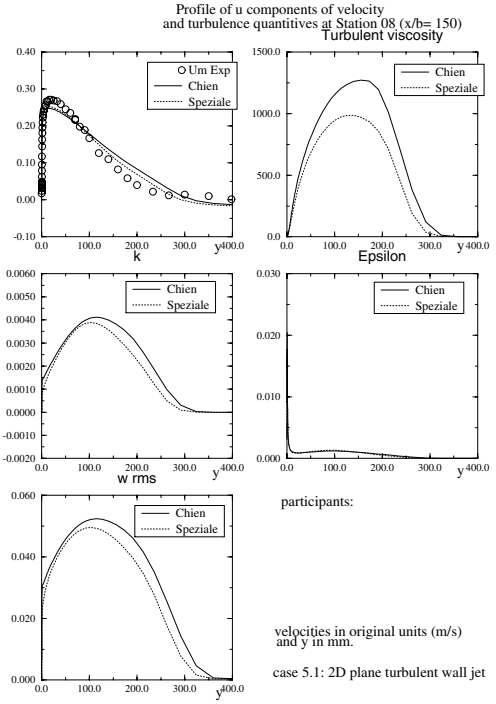

participants:

velocities in original units (m/s)
and y in mm.

case 5.1: 2D plane turbulent wall jet

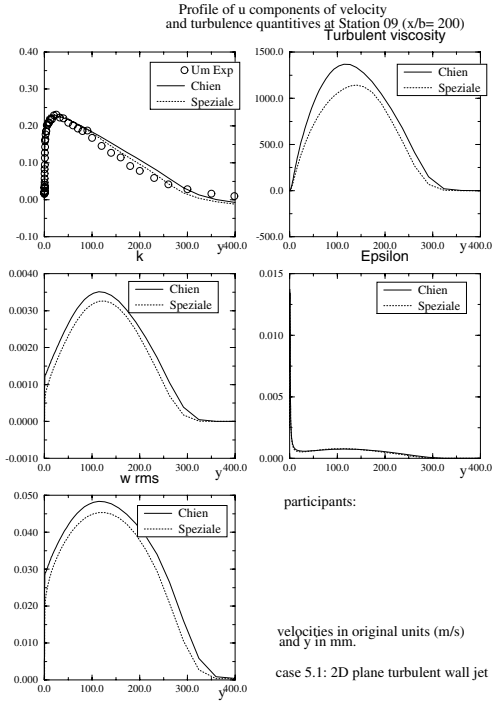

participants:

velocities in original units (m/s)
and y in mm.

case 5.1: 2D plane turbulent wall jet